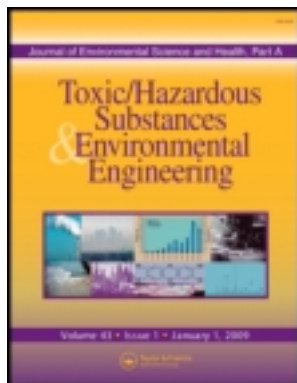


This article was downloaded by: [King Abdulaziz University]

On: 06 November 2013, At: 20:53

Publisher: Taylor & Francis

Informa Ltd Registered in England and Wales Registered Number: 1072954 Registered office: Mortimer House, 37-41 Mortimer Street, London W1T 3JH, UK



Journal of Environmental Science and Health, Part A: Toxic/Hazardous Substances and Environmental Engineering

Publication details, including instructions for authors and subscription information:

<http://www.tandfonline.com/loi/lesa20>

Synthesis, characterization and photocatalytic activity of $\text{Al}_2\text{O}_3\text{-TiO}_2$ based composites

Zulfiqar Ali ^{a b}, M. Aslam ^c, Iqbal M.I. Ismail ^{c d}, A. Hameed ^{b c}, Syed Tajammul Hussain ^b, Muhammad Nawaz Chaudhry ^a & M.A. Gondal ^e

^a College of Earth & Environmental Sciences, University of the Punjab, Lahore, Pakistan

^b National Centre for Physics, Quaid-e-Azam University, Islamabad, Pakistan

^c Center of Excellence in Environmental Studies, King Abdulaziz University, Jeddah, Saudi Arabia

^d Chemistry Department, Faculty of Science, King Abdulaziz University, Jeddah, Saudi Arabia

^e Department of Physics, King Fahd University of Petroleum and Minerals, Dhahran, Saudi Arabia

Published online: 11 Oct 2013.

To cite this article: Zulfiqar Ali, M. Aslam, Iqbal M.I. Ismail, A. Hameed, Syed Tajammul Hussain, Muhammad Nawaz Chaudhry & M.A. Gondal (2014) Synthesis, characterization and photocatalytic activity of $\text{Al}_2\text{O}_3\text{-TiO}_2$ based composites, Journal of Environmental Science and Health, Part A: Toxic/Hazardous Substances and Environmental Engineering, 49:1, 125-134, DOI: [10.1080/10934529.2013.824789](https://doi.org/10.1080/10934529.2013.824789)

To link to this article: <http://dx.doi.org/10.1080/10934529.2013.824789>

PLEASE SCROLL DOWN FOR ARTICLE

Taylor & Francis makes every effort to ensure the accuracy of all the information (the "Content") contained in the publications on our platform. However, Taylor & Francis, our agents, and our licensors make no representations or warranties whatsoever as to the accuracy, completeness, or suitability for any purpose of the Content. Any opinions and views expressed in this publication are the opinions and views of the authors, and are not the views of or endorsed by Taylor & Francis. The accuracy of the Content should not be relied upon and should be independently verified with primary sources of information. Taylor and Francis shall not be liable for any losses, actions, claims, proceedings, demands, costs, expenses, damages, and other liabilities whatsoever or howsoever caused arising directly or indirectly in connection with, in relation to or arising out of the use of the Content.

This article may be used for research, teaching, and private study purposes. Any substantial or systematic reproduction, redistribution, reselling, loan, sub-licensing, systematic supply, or distribution in any form to anyone is expressly forbidden. Terms & Conditions of access and use can be found at <http://www.tandfonline.com/page/terms-and-conditions>

Synthesis, characterization and photocatalytic activity of Al₂O₃-TiO₂ based composites

ZULFIQAR ALI^{1,2}, M. ASLAM³, IQBAL M.I. ISMAIL^{3,4}, A. HAMEED^{2,3}, SYED TAJAMMUL HUSSAIN², MUHAMMAD NAWAZ CHAUDHRY¹ and M.A. GONDAL⁵

¹College of Earth & Environmental Sciences, University of the Punjab, Lahore, Pakistan

²National Centre for Physics, Quaid-e-Azam University, Islamabad, Pakistan

³Center of Excellence in Environmental Studies, King Abdulaziz University, Jeddah, Saudi Arabia

⁴Chemistry Department, Faculty of Science, King Abdulaziz University, Jeddah, Saudi Arabia

⁵Department of Physics, King Fahd University of Petroleum and Minerals, Dhahran, Saudi Arabia

The synthesis, characterization and photocatalytic performance of non-traditional Al₂O₃-TiO₂-based photocatalysts is reported. Al₂O₃-TiO₂ support was loaded with various fractions of CuO and ZrO₂. A sound agreement was observed between the bandgaps of synthesized powders measured by UV-Visible diffuse reflectance spectroscopy (DRS) in the solid phase and UV-Visible spectroscopy in the aqueous medium. X-ray diffraction (XRD) analysis revealed the composite nature of the catalysts with the retention of individual identity of each component. The average crystallite size of the individual component was found to be in the range of 20 to 40 nm. Scanning electron microscopy (SEM) analysis authenticated the presence of CuO and ZrO₂ at the surface of Al₂O₃-TiO₂ support, while Rutherford Back Scattering Spectroscopy (RBS) confirmed the quantity of the modifiers as per theoretical calculations. The composites showed an enhanced photocatalytic activity in sunlight compared to Al₂O₃-TiO₂ for the degradation of dyes. Efforts were made to elucidate the enhanced sunlight response of the synthesized composite catalysts compared to Al₂O₃-TiO₂. As monitored by ion chromatography (IC), the synthesized photocatalysts completely mineralized the dyes leaving behind inorganic ions in solution. The kinetics of photocatalytic degradation of dyes was evaluated for optimum correlation with the existing models. The stability of the photocatalysts against the photo-corrosion was monitored by analyzing the samples for respective metals in solution after sunlight exposure.

Supplemental materials are available for this article. Go to the publisher's online edition of the *Journal of Environmental Science and Health, Part A*, to view the supplemental file.

Keywords: Dyes, composites, photocatalysis, photocorrosion, sunlight.

Introduction

Sunlight photocatalysed water decontamination leading to the complete oxidation of organic contaminants is considered as an economically viable option for water purification in the future.^[1–10] Although TiO₂ is the most suitable and widely studied photocatalyst for the degradation of variety of contaminants in water, owing to wide bandgap of 3.2 eV. Hence its activity is limited as it can harvest only 3% of the total sunlight.^[11,12] There is a great demand to enhance its activity in natural sunlight by applying suitable surface modification without losing its inherent activity.

Among the other existing surface modification techniques, TiO₂-based mixed oxide composites have proved to be the efficient photocatalysts in the visible region.^[13,14] A number of papers are reported recently to enhance the response of TiO₂ to solar spectrum using SnO₂, ZnO and ZrO₂ as surface modifiers.^[15–22] Our previous studies with wide bandgap semiconductors such as ZnO and NiO proved that the composite formation is a suitable tool for enhancing the photocatalytic performance.^[23–26] However the choice of suitable surface modifier and its compatibility with the base material in terms of its physical, chemical and optical properties is essential.^[27–32]

Al₂O₃, besides its use in enhancing the spectral response, photocatalytic activity and solar energy conversion of TiO₂,^[33–36] is well known for its adsorption ability due to exchangeable ions at the surface. The presence of insulating layers of Al₂O₃ at the surface of TiO₂ suppresses the unwanted charge recombination, thus enhancing the photocatalytic activity.^[33] ZrO₂ is a wide bandgap ($E_g =$

Address correspondence to M.A. Gondal, Department of Physics, King Fahd University of Petroleum & Minerals, Box 372, Dhahran 31261, Saudi Arabia; E-mail: magondal@kfupm.edu.sa

Received May 23, 2013.

4.5eV) semiconductor with a diverse use in the ceramic industry. A number of researchers have reported an enhanced photocatalytic activity of TiO₂ when modified with ZrO₂ as it alters the band gap leading to a greater absorption of light in the visible spectral region^[37,38] CuO is a visible light responsive p-type semiconductor with a bandgap of 1.7eV.^[39]

The presence of CuO at the surface of TiO₂ induces the interfacial electron transfer, thus suppressing the charge carrier recombination process for enhanced photocatalytic activity and spectral response. As CuO is an electron deficient p-type semiconductor, it acts as a sink for photogenerated electrons.^[40]

In the present study, owing to the established role of CuO, ZrO₂ and Al₂O₃ in photocatalysis, Al₂O₃-TiO₂ (5% Al₂O₃)-based four composites were synthesized by varying the ratios of CuO and ZrO₂. The photocatalytic activities of synthesized composite photocatalysts were evaluated in sunlight for the degradation of dyes, namely Direct Sky Blue 5B (DSB), Congo Red (CR), Alizarine Yellow (AY), Indigo Carmine (IC) and Rose Bengal (RB). The dyes were selected on the basis of their absorption spectra, λ_{\max} and the extent of absorption band so as to evaluate the contribution of indirect charge transfer photocatalysis induced by the dye molecules along with direct photocatalysis.

Materials and methods

Synthesis of CuO-ZrO₂-Al₂O₃-TiO₂ composites

CuO-ZrO₂@Al₂O₃-TiO₂ composites were synthesized by a co-precipitation sedimentation method, using ammonium carbonate as a precipitating agent, in two steps.^[41] In the first step, Al₂O₃-TiO₂ support was synthesized by suspending the appropriate amount of TiO₂ (Merck, Darmstadt, Germany, 99.99%) in 500 mL of deionized water and homogenized for 30 min under stirring. The dissolved stoichiometric amount of Al (NO₃)₃·9H₂O (Sigma-Aldrich, St. Louis, MO, USA, 99.99%) was added to TiO₂ suspension and precipitated by a drop-wise addition of (NH₄)₂CO₃. The slurry was aged overnight with continuous stirring at room temperature. The resultant precipitates, after drying at 100°C overnight, were calcined at 400°C for 4 h. The CuO and ZrO₂ loaded Al₂O₃-TiO₂ composites were synthesized by using the respective metal nitrates and appropriate amounts of Al₂O₃-TiO₂. The compositions and designated identifications of the synthesized catalysts are listed in Table 1.

Characterization of CuO-ZrO₂@Al₂O₃-TiO₂ composites

The bandgaps of synthesized composite powders were determined by UV/Visible diffused reflectance spectroscopy (DRS) in the solid state phase and UV-Visible spectroscopy in the aqueous phase. The XRD patterns of the synthesized

Table 1. Identity and composition of synthesized composite photocatalysts.

Identity	Composition
ZA-I	5% CuO-20%-ZrO ₂ @5% Al ₂ O ₃ -70% TiO ₂
ZA-II	10% CuO-15% ZrO ₂ @5% Al ₂ O ₃ -70% TiO ₂
ZA-III	15% CuO-10% ZrO ₂ @5% Al ₂ O ₃ -70% TiO ₂
ZA-IV	20% CuO-5% ZrO ₂ @5% Al ₂ O ₃ -70% TiO ₂

powders were acquired using a Scintag (Cupertino, CA, USA) XDS 2000 diffractometer, equipped with a Cu-K α radiation source. The crystallite sizes of various phases were calculated by applying Scherer's equation to the main reflection peaks of the respective XRD pattern. The Field Emission Scanning Electron Microscope (JEOL, Tokyo, Japan, JSM 6490-A) was applied to investigate the morphology of synthesized composites. Rutherford backscattering spectrometry (RBS) was employed for the elemental analysis and distribution of modifier metal. A collimated 2.0-MeV He²⁺ beam 20 nA and 20 μ C of 5-mm diameter produced by Tandem Pelletron Accelerator (SUDH-2, National Electrostatic Corporation, Middleton, WI, USA), was used for RBS measurements. The XPS spectra of synthesized composites were obtained by a wide survey scan between 0 to 1000 eV binding energies using an X-ray Photoelectron Spectrometer (PHI 5000 Versa Prob II, ULVAC-PHI Inc., Kanagawa, Japan).

The photocatalytic degradation of dyes (50 mgL⁻¹) was studied in the aqueous medium. The catalyst/dye suspension (100 mg/100 mL) was exposed to focused sunlight in a Pyrex[®] glass reactor with stirring. The degradation process was monitored by analyzing the samples, drawn at regular intervals, using UV-Visible spectrophotometer (Shimadzu, Kyoto, Japan, UV-1800). The amount of the catalyst was optimized by exposing the varying amounts of catalyst for a fixed exposure time. The photocatalytic activity of individual dye was evaluated by performing the experiments with pure CuO, ZrO₂ and Al₂O₃-TiO₂. The role of direct photolysis in dye degradation was estimated by exposing the dye solution to sunlight for 1 h without a catalyst. The adsorption of dyes on different catalysts was evaluated by performing the reaction in the dark. The progress of mineralization was observed by measuring the expected anions in selected samples by ion chromatograph (Shimadzu HIC-20A).

Results and discussion

Absorption spectra and bandgap evaluation

The absorption spectra of the synthesized powders were recorded by suspending them in the aqueous medium. The absorption edge of the valence band was identified by extrapolating the curves obtained by plotting the photon

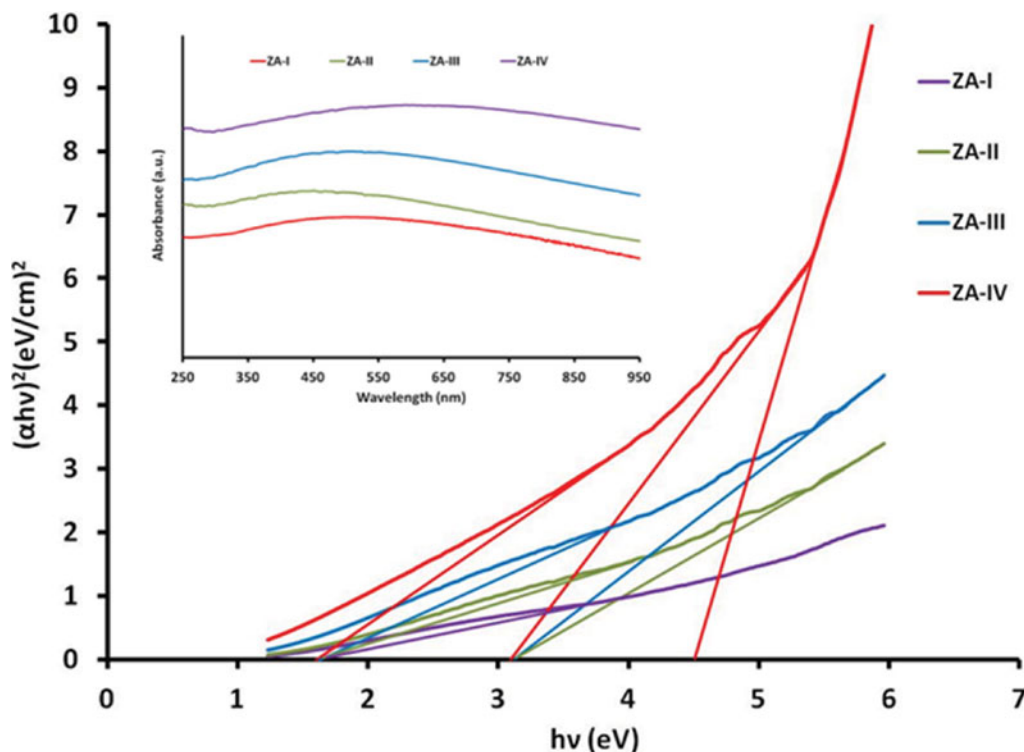


Fig. 1. Graphical determination of bandgaps of Al₂O₃-TiO₂ and synthesized composites by extrapolating $h\nu$ versus $(\alpha h\nu)^2$ curves to x-axis. The onset shows the absorption spectra of Al₂O₃-TiO₂ and synthesized composites in the aqueous medium (color figure available online).

energy ($h\nu$) versus $(\alpha h\nu)^2$ while “ α ” was evaluated by using the following equation.^[42–44]

$$\alpha = \frac{1}{l} \frac{A}{\log e} = \frac{1}{l} \frac{A}{2.303} (\text{cm}^{-1})$$

The absorption spectra and the graphical evaluation of the bandgaps of synthesized powders are presented in Figure 1, showing an enhanced absorption in the visible region with the increasing concentration of CuO can be observed. For ZA-I, all the three absorbing components, i.e., CuO, TiO₂ and ZrO₂, with the band gaps of 1.65, 3.1 and 4.5 eV, respectively, were identified, yet for ZA-II and ZA-III only the absorption bands of CuO and TiO₂ were identified revealing the suppression of photon absorption with increasing ZrO₂ concentration. The absence of bandgaps of TiO₂ and ZrO₂ for ZA-IV clearly predicts the complete surface coverage by CuO particles.

To validate the above-mentioned procedure, the bandgaps of the synthesized powders were evaluated by solid state diffuse reflectance spectroscopy. The band gap analysis plots of Kubelka–Munk (K-M) function versus photon energy ($h\nu$) are depicted in Figure 2. The comparison of the bandgaps in the solid and aqueous phase is presented in Table 2, showing that both procedures are equally suitable for the evaluation of bandgaps of the semiconductor powders. The minor shifts of the bandgaps towards either the higher or lower wavelengths are due to

enhanced $d-d$ and charge transfer transitions in the solid phase compared to the aqueous medium.

Structural and morphological characterization

A comparison of XRD patterns of the synthesized composite photocatalysts is depicted in Figure 3, where it can be observed that the reflections arising from TiO₂ are dominant in the XRD patterns of all the four composites. The reflections at 2θ positions of 26.634, 32.281 and 74.398 confirmed the presence of CuO phase (JCPDS-34-1354). Similarly, the reflections at 2θ positions of 35.190 and 67.883 matched those of Al₂O₃ (JCPDS-34-0493). Low intensity

Table 2. Comparison of bandgaps evaluated by UV-Visible (DRS) and UV-Visible spectroscopy.

Catalyst	UV-Visible DRS spectroscopy (Solid phase)			UV-Visible spectroscopy (Liquid phase)		
	TiO ₂	CuO	ZrO ₂	TiO ₂	CuO	ZrO ₂
ZA-I	3.3 eV	1.45 eV	3.9	3.2	1.6	4.5
ZA-II	3.0 eV	1.45 eV	3.9	3.1	1.65	—
ZA-III	3.1 eV	1.5 eV	3.9	3.1	1.65	—
ZA-IV	3.2 eV	1.5 eV	3.9	—	1.65	—

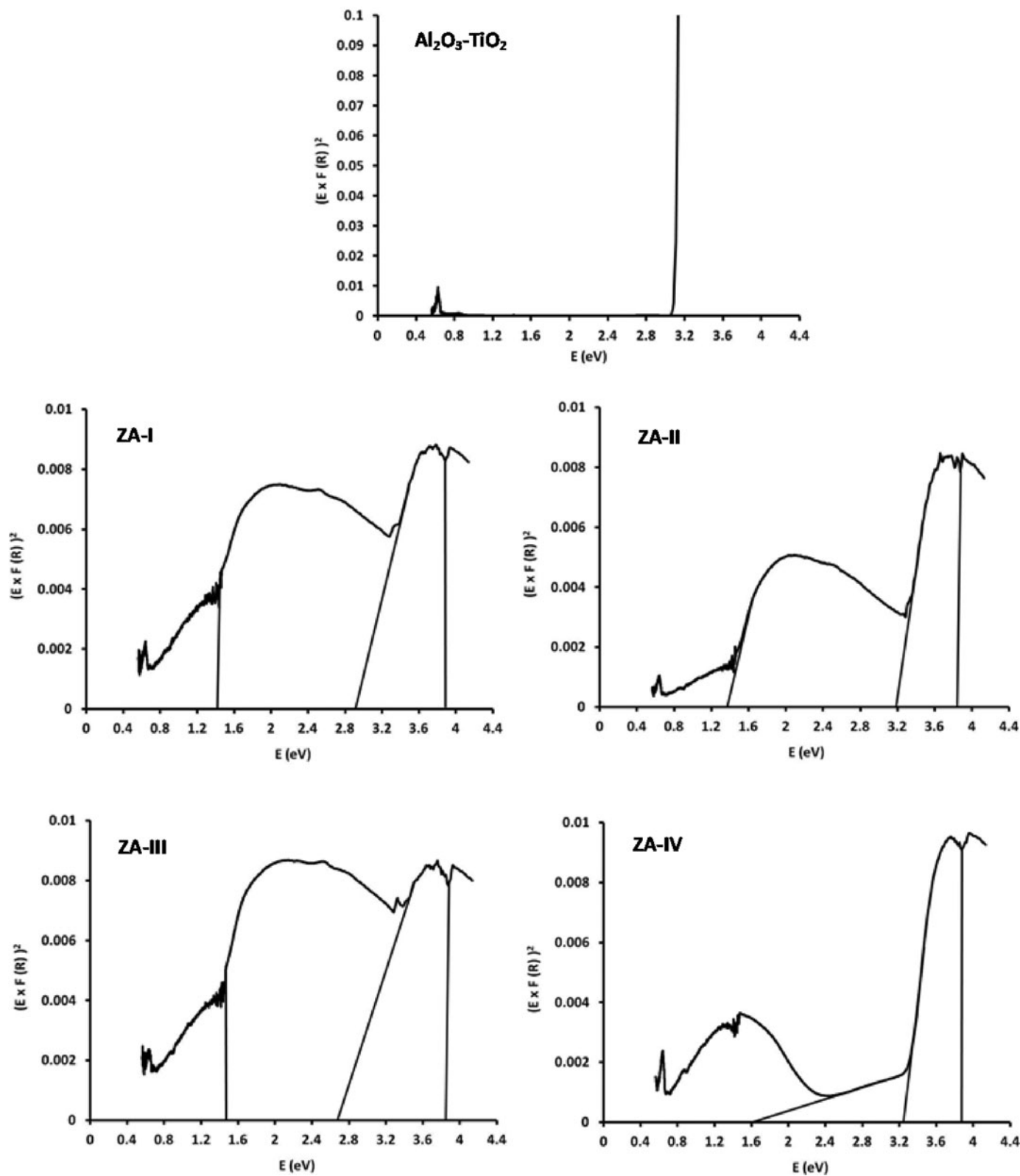


Fig. 2. Graphical determination of bandgaps of $\text{Al}_2\text{O}_3\text{-TiO}_2$ and synthesized composites by extrapolating E versus $(E \times F(R))^2$ curves to x-axis where $F(R)$ are derived from the diffuse reflectance spectra of $\text{Al}_2\text{O}_3\text{-TiO}_2$ and synthesized composites in the solid state.

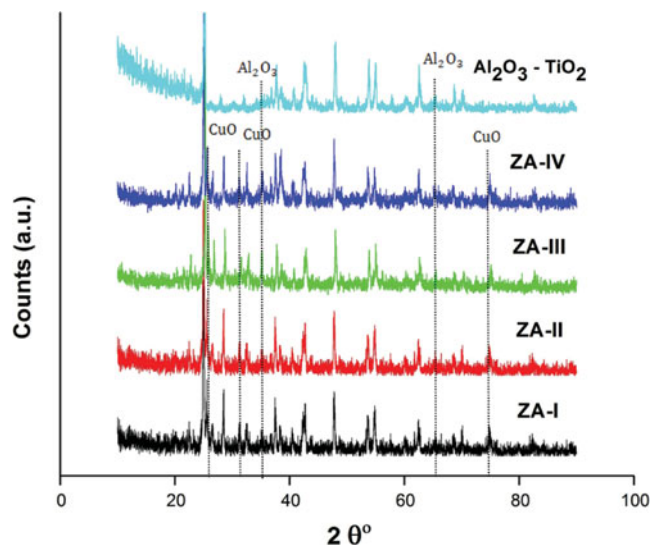


Fig. 3. Comparison of the XRD pattern of $\text{Al}_2\text{O}_3\text{-TiO}_2$ with that of synthesized powders (color figure available online).

peaks at the 2θ positions of 38.362, 60.05 and 70.369 were identical to the standard pattern of ZrO_2 (JCPDS-17-0385). The average crystal sizes of all the phases, as calculated by Scherrer's equation using FWHM values of the most intense peaks, were 26 nm, 29 nm, 32 nm and 37 nm for ZA-I, ZA-II, ZA-III and ZA-IV, respectively. The increase in the crystallite size with increasing the concentration of CuO reflects the enhanced surface coverage or formation of CuO aggregates at the surface.

As presented in Figure 4, the morphology of synthesized powders was evaluated by FESEM. The fibrous nano-aggregates of ZrO_2 , which shrink with the decreasing concentration of ZrO_2 from ZA-I to ZA-IV, can be clearly seen in all the micrographs. It was observed that the CuO loading has no significant effect on the morphology of TiO_2 . A mild increase in the particle size can be observed with increasing the concentration of CuO , which is in accordance with XRD finding as metal oxides can modulate the surface of the catalyst by enhancing the dispersion of active sites. The RBS spectra of the synthesized powders are

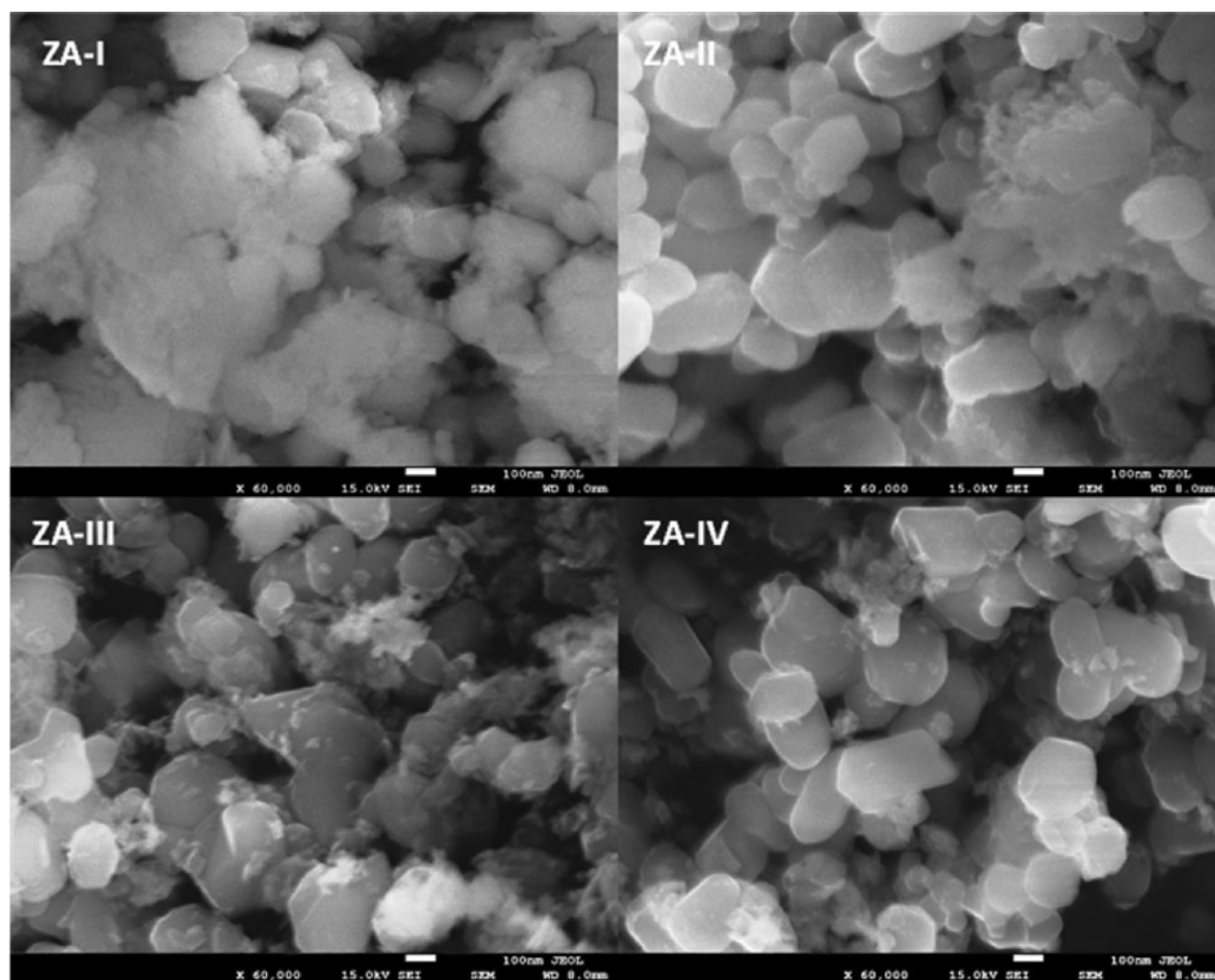


Fig. 4. FESEM images of synthesized composites; ZA-I (5% CuO -20%- ZrO_2 @5% Al_2O_3 -70% TiO_2), ZA-II (10% CuO -15% ZrO_2 @5% Al_2O_3 -70% TiO_2), ZA-III (15% CuO -10% ZrO_2 @5% Al_2O_3 -70% TiO_2) and ZA-IV (20% CuO -5% ZrO_2 @5% Al_2O_3 -70% TiO_2).

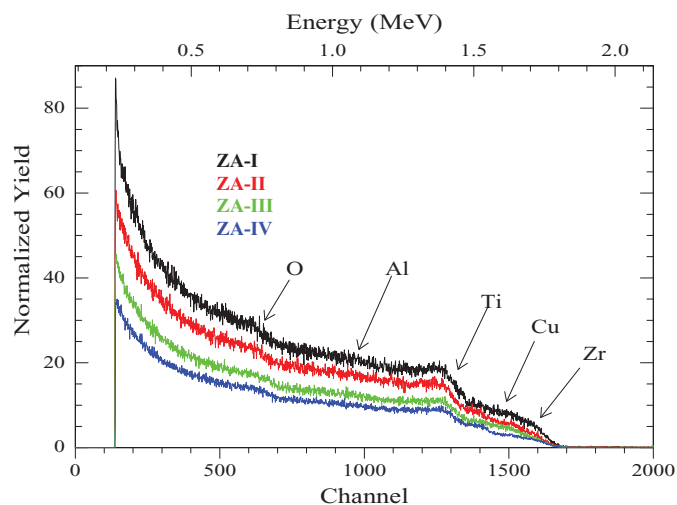


Fig. 5. Rutherford Back Scattering (RBS) spectra of synthesized Al_2O_3 - TiO_2 -based composites (color figure available online).

presented in Figure 5, which confirmed the homogeneous layer deposition of surface modifiers without irregularities.

The comparison of XPS survey scans of the synthesized composites is presented in Figure 6, where an increase in the $\text{Cu}2p_1$ and $\text{Cu}2p_3$ peaks at 952.8 eV and 933.6 eV, representing the +2 oxidation state of Cu, can be observed from ZA-I to ZA-IV. Similarly a decrease in the intensity of $\text{Zr}3d$ peak at 183.2 eV can be observed with the decreasing concentration of ZrO_2 at the surface from ZA-I to ZA-IV. The binding energy of 183.2 eV, although shifted to a higher value due to the matrix effect, depicts +4 oxidation state of Zr in the form of ZrO_2 .

The intense peak of $\text{Ti}2p$ was observed at a binding energy of 458.7 eV, which is in good agreement with the standard binding energy (458.68 eV) of TiO_2 , while $\text{Al}2p$ peak in synthesized composites observed at the binding energy

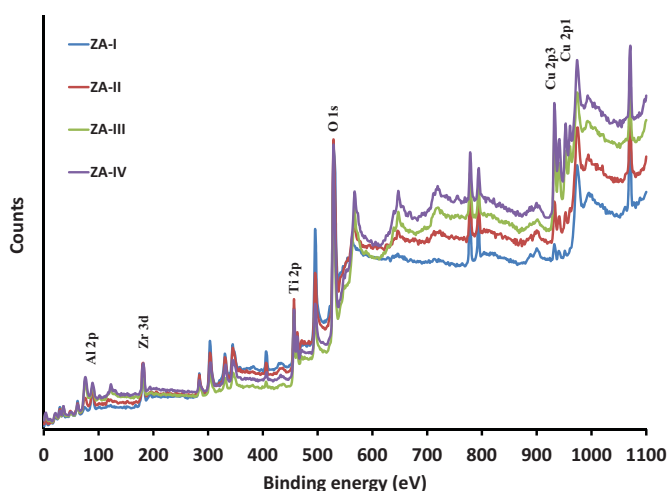
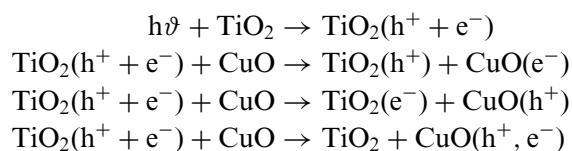


Fig. 6. XPS survey scan of the synthesized composites (color figure available online).

of 76.0 eV, which shows that Al occurs in the +3 oxidation state in the form of Al_2O_3 . As expected, the $\text{O}1s$ peak appears at the binding energy of 528.8 eV. Due to the complex nature of matrix in the composites, a mild shift in some of the binding energies, compared to standard values, was observed, which is acceptable in multi-oxide complex systems.

Photocatalytic performance of synthesized composites

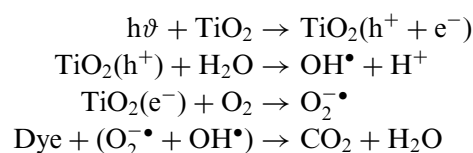
For TiO_2 , the high charge recombination rate and shorter life span of excited states (10^{-9} - 10^{-12} s), suppresses the formation of oxidizing species.^[12] Also the wide bandgap of 3.2 eV restricts the absorption of photons in the visible spectrum, i.e., $E_{\text{photon}} \leq 380$ nm that limits its use in the sunlight with the major portion of light in the visible region. The issue of recombination inhibition and light harvesting in the visible region can be tackled via modifying the surface of a wide bandgap photocatalyst by composite formation, which induces the charge separation through the interfacial charge transfer between the allowed energy states. A possible mechanism of charge carriers trapping with respect to TiO_2 in the synthesized composites can be elaborated by the following set of equations:

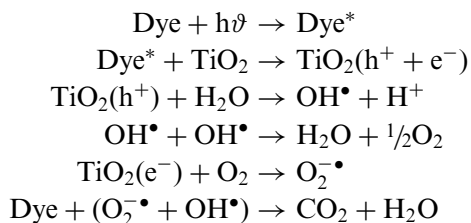


In the present study, it was observed that the presence of Al_2O_3 , a non-semiconductor, enhanced the adsorption of dyes on the composites. It is important to mention here that apart from enhancing the adsorption of dyes, no significant role of Al_2O_3 in either enhancing or suppressing the photodegradation process both in composites and Al_2O_3 - TiO_2 support was observed.

In photocatalytic degradation processes, the degradation of dyes is accomplished by two plausible modes namely; direct and charge transfer indirect photocatalysis. Direct photocatalytic degradation of dyes proceeds through the oxidation of dyes by the oxidizing species generated as a result of a direct bandgap excitation of the semiconductor photocatalyst, yet in the indirect charge transfer photocatalysis, the oxidizing species are generated by dye assisted energy injection to the valence band of photocatalyst. The two modes of photocatalytic dye degradation can be represented by the following equations:

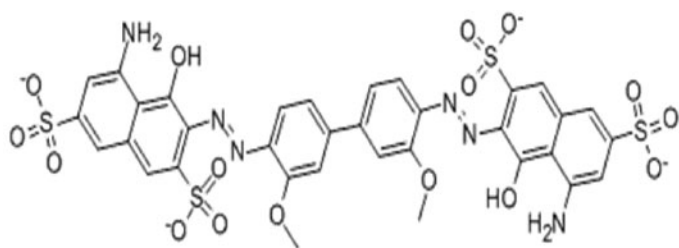
Direct photocatalysis



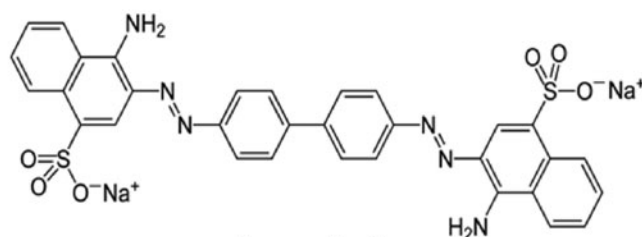
Indirect charge transfer photocatalysis

In the present study the choice of the dye is based on their absorption spectra so as to evaluate the contribution of direct and indirect photocatalysis in the dye degradation process. Among the selected dyes only Rose Bengal (RB) does not possess any strong absorption band in the absorption region of TiO₂, i.e., 200-400 nm, while the rest of the dyes possess strong absorption band in the same region. The percentage of the dye degraded as a function of time was evaluated using the relation as mentioned here.

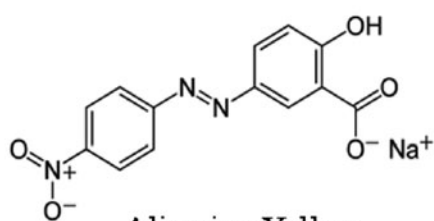
$$\text{Degradation (\%)} = \frac{(C_t - C_o)}{C_o} \times 100 = \frac{(A_t - A_o)}{A_o} \times 100$$



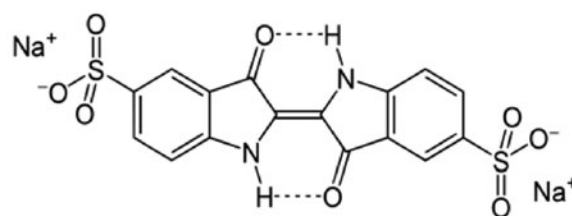
Direct Sky Blue 5B



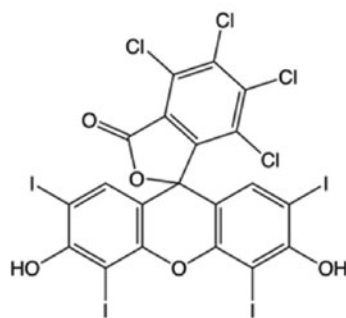
Congo Red



Alizarine Yellow



Indigo Carmine



Rose Bengal

where C_o and C_t are the concentrations, while A_o and A_t are the absorbance values of the dye solution before and after irradiation, respectively.

Photocatalytic degradation of dyes

The structures of the dyes used to investigate the photocatalytic performance of the synthesized composites are presented in Scheme 1.

Direct Sky Blue 5B is an azo dye with two absorption bands at λ = 598 nm and λ = 313 nm. The high intensity band with λ_{max} = 598 nm wraps a region of 700–500 nm while the low intensity band at λ_{max} = 313 nm covers a region of 370–260 nm. The low degradation response of Al₂O₃-TiO₂ is mainly due to the fact that it can utilize only 3% of solar spectrum. Additionally the presence of low intensity band of DSB in the 370–260 nm region sweeps a significant number of photons, making these inaccessible to TiO₂, thus causing a significant decrease in dye degradation. The observed degradation seems to be arising due to indirect photocatalysis initiated by the dye molecules.

Scheme 1. Structure of dyes.

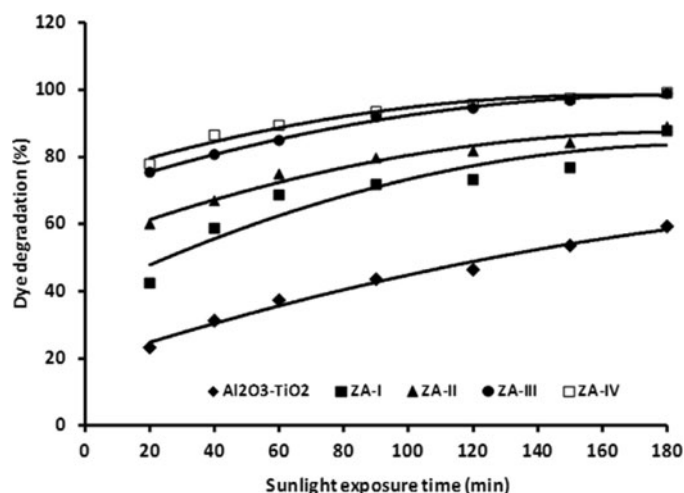


Fig. 7. Representative plot for the comparison of percentage degradation of DSB 5B over Al₂O₃-TiO₂ and synthesized composites.

For the four composites, the degradation increased sharply with increasing the concentration of CuO, which shows that both direct and indirect modes are operative simultaneously for the dye degradation as CuO with a bandgap of ~ 1.7 eV can absorb the photons having energy even below 700 nm. Also the energy transfer from excited dye molecules to CuO for the induction of charge separation for enhanced generation of excited species to degrade the dye cannot be ruled out. No appreciable role of ZrO₂ for enhancing the degradation process was observed. The analysis revealed that the degradation of DSB for Al₂O₃-TiO₂ is $\sim 59\%$, which is comparatively low when compared with ZA-I ($\sim 87\%$), ZA-II ($\sim 89\%$), ZA-III ($\sim 98\%$) and ZA-IV ($\sim 99\%$) under sunlight exposure in 180 min as shown in Figure 7.

The degradation behavior of Congo Red (CR) was even more complex compared to DSB 5B as a low degradation of the dye was observed for Al₂O₃-TiO₂. CR, an azo dye, possesses two strong absorption bands, at $\lambda_{\max} = 495$ nm and at $\lambda_{\max} = 346$ nm. The band at $\lambda_{\max} = 346$ nm covers 400–280 nm region of the spectrum, which is the main photon absorption area of TiO₂. The absorption of appreciable number of photons by the dye molecules in this region (400–280 nm) causes a significant decrease in the activity of TiO₂. The decreased activity of Al₂O₃-TiO₂ for the degradation of CR also indicated the decreased extent of indirect photocatalysis by the excited dye molecules.

To investigate the plausible causes, experiments were performed with the dye under the same conditions but without a photocatalyst. A higher extent of dye degradation, $\sim 28\%$, as a result of direct photolysis, was observed in CR compared to that of DSB 5B indicating that the absorbed photons in the UV region are consumed by the dye itself for self fragmentation rather than transferring to TiO₂, thus causing a significant decrease in the photocatalytic degra-

degradation by TiO₂. All the synthesized catalysts showed a superior activity in sunlight exposure and $\sim 86\%$, $\sim 92\%$, $\sim 96\%$ and $\sim 99\%$ degradation was observed for ZA-I, ZA-II, ZA-III and ZA-IV, respectively, compared to $\sim 32\%$ for pure Al₂O₃-TiO₂ in 180 min, as shown in Figure S1 (Supplementary Information). The increased activity of the composites is owing to their ability of harvesting the photons in the visible region even in the presence of strong absorption by the dye molecules.

Alizarine Yellow (AY) is an azo dye with a strong absorption band between 500–700 nm with $\lambda_{\max} = 352.5$ nm, which predicts a complete coverage of the absorption region of TiO₂. The low degradation of this dye over the Al₂O₃-TiO₂ base, i.e., $\sim 25\%$ in 180 min, was observed despite the fact that the only available mode of degradation is charge transfer photocatalysis rather than direct photocatalysis. The observed low degradation, $\sim 8\%$ in 180 min, of this dye by direct photolysis supports this finding. For composites, the dye degradation gradually increases with the increase in surface population density of CuO. The percentage degradation of $\sim 58\%$, $\sim 63\%$, $\sim 74\%$ and $\sim 78\%$ was observed for ZA-I, ZA-II, ZA-III and ZA-IV, respectively, as shown in Figure S2 (Supplementary Information).

Indigo Carmine (IC), an anionic dye with intramolecular hydrogen bonding, possesses two strong absorption bands between 500–700 nm with λ_{\max} at 610 nm and the second band between 200–400 nm. Despite the coverage of the excitation region of TiO₂ by the dye, a significantly high degradation, $\sim 83\%$ in 180 min, was observed for the Al₂O₃-TiO₂ base revealing the enhanced extent of charge transfer photocatalysis. For the synthesized composites, an increased degradation of $\geq 95\%$ were observed, which is shown in Figure S3 (Supplementary Information) suggesting charge separation synergy between TiO₂ and CuO.

Rose Bengal (RB), a halogenated phenolic dye, possesses only one strong absorption band between 500–600 nm with λ_{\max} at ~ 556 nm, while the rest of the region between 200–500 nm is available for TiO₂ absorption. For Al₂O₃-TiO₂, a significantly high degradation efficiency, i.e., $\sim 83\%$ in 180 min, was observed, which is inherent for TiO₂. For composites, the degradation decreases with the increasing CuO contents suggesting the loss of charge transfer effect with increasing the surface density of CuO. Compared to 83% for Al₂O₃-TiO₂, the percentage degradation of RB was observed $\sim 93\%$, $\sim 92\%$, $\sim 88\%$ and $\sim 78\%$ for ZA-I, ZA-II, ZA-III and ZA-IV, respectively, as shown in Figure S4 (Supplementary Information).

Keeping in view the reaction conditions and the reactants involved, the kinetics of photocatalytic degradation of respective dyes were evaluated by applying various kinetic models. However, the best correlation of the degradation data was observed with pseudo-first-order kinetic model. The representative plot of $\ln(C_0/C)$ versus exposure time (t) for DSB 5B is presented in Figure 8 and the plots for the remaining dyes are provided in Figures S5–8 (Supplementary Information). A comparison of the

Table 3. Comparison of the evaluated kinetic parameters, rate constants (k_1) and correlation factors (R^2), for the degradation of dyes under sunlight irradiation.

Catalysts	Direct Sky Blue		Congo Red		Alizarin Yellow		Indigo Carmine		Rose Bengal	
	k_1 (min ⁻¹)	R^2								
Al ₂ O ₃ - TiO ₂	0.0037 ± 0.00049	0.98	0.0021 ± 0.00035	0.99	0.0015 ± 0.00028	0.97	0.010 ± 0.0028	0.99	0.011 ± 0.0021	0.99
ZA-I	0.0078 ± 0.00057	0.89	0.0099 ± 0.00042	0.98	0.0039 ± 0.00021	0.99	0.019 ± 0.0021	0.98	0.011 ± 0.0028	0.98
ZA-II	0.0074 ± 0.00042	0.96	0.011 ± 0.0028	0.97	0.0043 ± 0.00035	0.99	0.022 ± 0.0021	0.97	0.011 ± 0.0035	0.93
ZA-III	0.018 ± 0.0035	0.97	0.011 ± 0.0035	0.94	0.0066 ± 0.00028	0.99	0.027 ± 0.0035	0.93	0.010 ± 0.0021	0.98
ZA-IV	0.018 ± 0.0028	0.97	0.016 ± 0.0021	0.93	0.0079 ± 0.00042	0.99	0.032 ± 0.0021	0.98	0.0079 ± 0.00042	0.99

evaluated rate constants (k_1) and correlation factors (R^2) for the photodegradation of all dyes under the same conditions is provided in Table 3.

The stability of various components of composites was monitored by analyzing the solution samples using ICP-OES. All the samples were found to be stable against photocorrosion, while no decomposition of the catalyst was observed under sunlight exposure. The anions such as SO₄²⁻, NO₃⁻, Cl⁻ and I⁻ were identified by ion chromatography (IC) of the selected samples. The presence of CO₃²⁻ was also observed.

Comparison of the photocatalytic activity of individual components with composites

The assumption of enhanced photocatalytic activity in the composite form compared to individual components was verified by performing the experiments with the individual pure components. The photocatalytic degradation activity of Al₂O₃-TiO₂ was discussed in detail previously. As expected, Al₂O₃ did not show any photocatalytic activity for the degradation of the dyes, however, as verified by performing the experiments in the dark, a significant dye adsorption was observed. Although a semiconductor in na-

ture, probably due to its wide bandgap, ZrO₂ failed to show any activity for dye degradation in sunlight. Pure CuO, although showed the photocatalytic activity for the degradation in sunlight, however the extent of dye degradation was much lower than that of composites, which revealed the synergetic effect between the components of composites.

Conclusion

The study proved that the photocatalytic activity of TiO₂ can be enhanced by suitable tailoring of the band gap (absorbing surface). However, the optimum efficiency of the composite photocatalyst can be achieved by choosing suitable modifiers with compatible band structures, morphological phase and chemical characteristics to facilitate the photon initiated interfacial electron transfer between the allowed states of the semiconductors involved. From the photocatalytic degradation results, it can be concluded that different dyes contribute in the indirect excited state charge transfer photocatalysis to varying extent. More investigations are required to explore the exact mechanism of dye involvement in the charge transfer photocatalysis.

Acknowledgments

Iqbal M.I. Ismail, A. Hameed and M. Aslam are thankful to CEE S., KAU (Project no. 1/W/1433) and Ministry of Higher Education, KSA, for support. M.A. Gondal is thankful to KFUPM for supporting this work.

References

- [1] Nasuha, N.; Hameed, B.H.; Din, A.T.M. Rejected tea as a potential low cost adsorbent for the removal of methylene blue. *J. Hazard. Mater.* **2010**, *175*, 126–132.
- [2] Martin, M.J.; Artola, A.; Balaguer, M.D.; Rigola, M. Activated carbons developed from surplus sewage sludge for the removal of dyes from dilute aqueous solutions. *Chem. Eng. J.* **2003**, *94*, 231–239.
- [3] Rauf, M.A.; Qadri, S.M.; Ashraf, S.; Al-Mansoori, K.M. Adsorption studies of Toluidine Blue from aqueous solutions onto gypsum. *Chem. Eng. J.* **2009**, *150*(1), 90–95.
- [4] Ahmad, A.L.; Puasa, S.W. Reactive dyes decolourization from an aqueous solution by combined coagulation/micellar-enhanced ultrafiltration process. *Chem. Eng. J.* **2007**, *132*, 257–265.
- [5] Riera-Torres, M.; Gutiérrez-Bouzán, C.; Crespi, M. Combination of coagulation–flocculation and nanofiltration techniques for dye

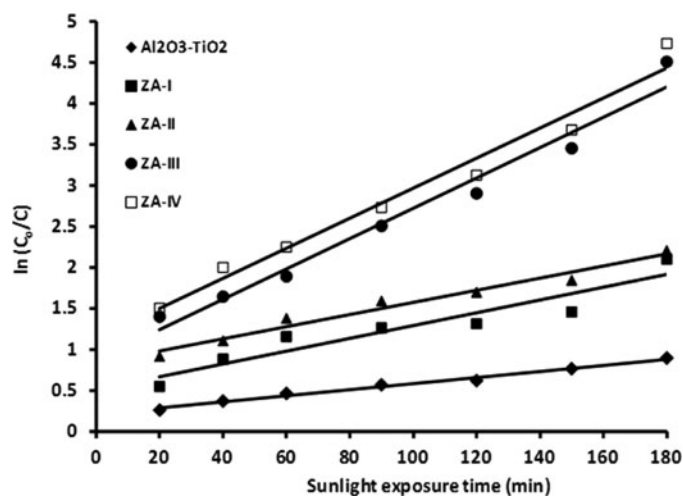


Fig. 8. Representative plot of $\ln(C_0/C)$ versus sunlight exposure time for the degradation of DSB 5B over Al₂O₃-TiO₂ and synthesized composites.

- removal and water reuse in textile effluents. *Desalination* **2010**, *252*, 53–59.
- [6] Shakir, K.; Elkafrawy, A.F.; Ghoneimy, H.F.; Elrab Beheir, S.G.; Refaat, M. Removal of rhodamine B (a basic dye) and thoron (an acidic dye) from dilute aqueous solutions and wastewater simulants by ion flotation. *Water Res.* **2010**, *44*, 1449–1461.
- [7] Zodi, S.; Potier, O.; Lopicque, F.; Leclerc, J.P. Treatment of the industrial wastewaters by electrocoagulation: Optimization of coupled electrochemical and sedimentation processes. *Desalination* **2010**, *261*(1–2), 186–190.
- [8] Ligrini, O.; Oliveos, E.; Braun, A. Photochemical processes for water treatment. *Chem. Rev.* **1993**, *93*, 671–698.
- [9] Rauf, M.A.; Ashraf, S.S. Application of Advanced Oxidation Processes (AOP) to dye degradation—an overview. In *Dyes and Pigments: New Research*; Lang, A.R., Ed.; Nova Science Publishers, Inc.: New York, 2009, 259–290.
- [10] Parsons, S. *Advanced Oxidation Processes for Water and Wastewater*; IWA Publishing: London, UK, 2004.
- [11] Fujishima, A.; Rao, T.N.; Tryk, D.A. Titanium dioxide photocatalysis. *J. Photochem. Photobiol. C Photochem. Rev.* **2000**, *1*, 1–21.
- [12] Hoffmann, M.R.; Martin, S.T.; Choi, W.Y.; Bahnemann, D.W. Environmental applications of semiconductor photocatalysis. *Chem. Rev.* **1995**, *95*, 69–96.
- [13] Kim, J.; Song, K.C.; Foncillas, S.; Pratsinis, S.E. Dopants for synthesis of stable bimodally porous titania. *J. Europ. Ceram. Soc.* **2001**, *21*, 2865–2874.
- [14] Manríquez, M.E.; López, T.; Gómez, R.; Navarrete, J. Preparation of TiO₂–ZrO₂ mixed oxides with controlled acid–basic properties. *J. Mol. Catal. A: Chem.* **2004**, *220*, 229–237.
- [15] Vinodgopal, K.; Kamat, P.V. Enhanced rates of photocatalytic degradation of an azo dye using SnO₂/TiO₂ coupled semiconductor thin films. *Environ. Sci. Technol.* **1995**, *29*, 841–845.
- [16] Neppolian, B.; Choi, H.C.; Sakthivel, S.; Arabindoo, B.; Murugesan, V. Solar/UV-induced photocatalytic degradation of three commercial textile dyes. *J. Hazard. Mater.* **2002**, *B89*, 303–317.
- [17] Lathasree, S.; Nageswara Rao, A.; Siva Sankar, B.; Sadasivam, V.; Rengaraj, K. Heterogeneous photocatalytic mineralization of phenols in aqueous solutions. *J. Mol. Catal. A.* **2004**, *223*, 101–105.
- [18] Lizama, C.; Freer, J.; Baeza, J.; Mansilla, H.D. Optimal photodegradation of reactive blue 9 on TiO₂ and ZnO suspension. *Catal. Today.* **2002**, *76*, 235–246.
- [19] Akyol, A.; Yatmaz, H.C.; Bayramoglu, M. Photocatalytic decolorization of Remazol Red RR in aqueous ZnO suspensions. *Appl. Catal. B: Environ.* **2004**, *54*, 19–24.
- [20] Cybulski, A.; Trawczyński, J. Catalytic wet air oxidation of phenol over platinum and ruthenium catalysts. *Appl. Catal. B: Environ.* **2004**, *47*, 1–14.
- [21] Wong, K.H.; Tao, S.; Dawson, R.; Wong, P.K. Optimization of photocatalytic oxidation of 2,2',3,3'-tetrachlorobiphenyl. *J. Hazard. Mater.* **2004**, *B109*, 149–155.
- [22] Yu, J.C.; Ho, W.; Yu, J.; Hark, S.K.; Lu, K. Effects of trifluoroacetic acid modification on the surface microstructures and photocatalytic activity of mesoporous TiO₂ thin films. *Langmuir* **2003**, *19*, 3889–3896.
- [23] Hameed, A.; Montini, T.; Gombac, V.; Fornasiero, P. Surface phases and photocatalytic activity correlation of Bi₂O₃/Bi₂O_{4-x} nanocomposite. *J. Am. Chem. Soc.* **2009**, *130*, 9658–9659.
- [24] Hameed, A.; Montini, T.; Gombac, V.; Fornasiero, P. Photocatalytic decolorization of dyes on NiO-ZnO nano-composites. *Photochem. Photobiol. Sci.* **2009**, *8*, 677–682.
- [25] Hameed, A.; Montini, T.; Gombac, V.; Fornasiero, P. Synthesis, characterization and photocatalytic activity of NiO-Bi₂O₃ nanocomposites. *Chem. Phys. Lett.* **2009**, *472*, 212–216.
- [26] Hameed, A.; Montini, T.; Gombac, V.; Fornasiero, P. Photocatalytic activity of zinc modified Bi₂O₃. *Chem. Phys. Lett.* **2009**, *483*, 254–261.
- [27] Gnatyuk, Yu.; Smirnova, N.; Eremenko, A.; Ilyin, V. Design and photocatalytic activity of mesoporous TiO₂/ZrO₂ thin films. *Adsorp. Sci. Technol.* **2005**, *23*, 497–508.
- [28] Fu, X.; Clark, L.A.; Yang, Q.; Anderson, M.A. The enhanced photocatalytic performance of titania-based binary metal oxides: TiO₂/SiO₂, TiO₂/ZrO₂. *Environ. Sci. Technol.* **1996**, *30*, 647–653.
- [29] Tseng, I.H.; Chang, W.C.; Wu, J.C.S. Photoreduction of CO₂ using sol-gel derived titania and titania-supported copper catalysts. *Appl. Catal. B: Environ.* **2002**, *37*, 37–48.
- [30] Tseng, I.H.; Wu, J.C.S. Chemical states of metal-loaded titania in the photoreduction of CO₂. *Catal. Today* **2004**, *97*, 113–119.
- [31] Li, G.H.; Dimitrijevic, N.M.; Chen, L.; Rajh, T.; Gray, K.A. The role of surface/interfacial Cu²⁺ sites in photocatalytic activity of coupled CuO-TiO₂ nanocomposites. *J. Phys. Chem. C* **2008**, *112*, 19040–19044.
- [32] Irie, H.; Kamiya, K.; Shibamura, T.; Miura, S.; Tryk, D.A.; Yokoyama, T.; Hashimoto, K. Visible lightsensitive Cu(II)-grafted TiO₂ photocatalysts: activities and x-ray absorption fine structure analyses. *J. Phys. Chem. C* **2009**, *113*, 10761–10766.
- [33] Granados-Correa, F.; Bulbulian, S. Surface characterization of γ -Al₂O₃ powders and their Co²⁺ adsorption properties. *Int. J. Appl. Ceram. Technol.* **2013**, *10*, 295–303.
- [34] Cai, W.; Yu, J.; Jaroniec, M. Template-Free synthesis of hierarchical spindle-like gamma-Alumina materials and their adsorption affinity towards organic and inorganic pollutants in water. *J. Mater. Chem.* **2010**, *20*, 4587–4594.
- [35] Trueba, M.; Trasatti, S.P. γ -Alumina as support for catalysts: A review of fundamental aspects. *Eur. J. Inorg. Chem.* **2005**, *17*, 3393–3403.
- [36] Vazquez, A.; Lopez, T.; Gomez, R.; Bokhimi, X.; Morales, A.; Novaro, O. X-ray diffraction, FTIR, and NMR characterization of sol-gel alumina doped with lanthanum and cerium. *J. Solid State Chem.* **1997**, *128*, 161–168.
- [37] Colón, G.; Hidalgo, M.C.; Navio, J.A. Effect of ZrO₂ incorporation and calcination temperature on the photocatalytic activity of commercial TiO₂ for salicylic acid and Cr(VI) photodegradation. *Appl. Catal. A: Gen.* **2002**, *231*, 185–199.
- [38] Corma, A. Inorganic solid acids and their use in acid-catalyzed hydrocarbon reactions. *Chem. Rev.* **1995**, *95*, 559–614.
- [39] Hui-li, X.; Hui-sheng, Z.; Tao, Z.; Dong-chang, X. Photocatalytic degradation of Acid Blue 62 over CuO-SnO₂ nanocomposite photocatalyst under simulated sunlight. *J. Environ. Sci.* **2007**, *19*, 1141–1145.
- [40] Chiang, K.; Amal, R.; Tran, T. Photocatalytic degradation of cyanide using titanium dioxide modified with copper oxide. *Adv. Environ. Res.* **2002**, *6*, 471–485.
- [41] Sun, K.P.; Lu, W.W.; Qiu, F.Y.; Xu, X.L. Direct synthesis of DME over bifunctional catalyst: surface properties and catalytic performance. *Appl. Catal. A.* **2003**, *252*, 243–249.
- [42] Dong, W.; Zhu, C. Optical properties of surface-modified Bi₂O₃ nanoparticles. *J. Phys. Chem. Sol.* **2003**, *64*, 265–271.
- [43] Yoffe, A.D. Low-dimensional systems: quantum size effects and electronic properties of semiconductor microcrystallites (zero-dimensional systems) and some quasi-two-dimensional systems. *Adv. Phys.* **1993**, *42*(2), 173–262.
- [44] Dong, W.T.; Wu, S.X.; Chen, D.P.; Jiang, X.W.; Zhu, C.S. Preparation of α -Fe₂O₃ nanoparticles by sol-gel process with inorganic iron salt. *Chem. Lett.* **2000**, *5*, 496–497.